Viral manipulation of functionally distinct neurons from mice to humans

Vormstein-Schneider DC [1] *, Lin JD [1] *, Pelkey KA [4], Chittajallu R [4], Guo B [1], Arias Garcia M [1], Sakopoulos S [1], Stevenson O [1], Schneider G [1], Zhang Q [6], Sharma J [6], Franken TP [7], Smith J [7], Vogel I [1], Sanchez V [1], Ibrahim LA [1,2], Burbridge T [1,2], Favuzzi E [1,2], Saldi GA [1,3], Xu Q [3], Guo L [3], Yuan X [4], Zaghloul KA [5], Sabri E [9], Goldberg EM [10], Devinsky O [8], Batista-Brito R [9], Reynolds J [7], Feng G [1,6], Fu Z [1], McBain CJ [4], Fishell GJ [1,2], Dimidschstein J [1] +

* These authors contributed equally to the work.
+ Corresponding author - email: jordane@broadinstitute.org

(1) Stanley Center for Psychiatric Research, Broad Institute of Harvard and MIT, Cambridge, MA, USA; (2) Department of Neurobiology at Harvard Medical School, Boston, MA, USA; (3) Center for Genomics & Systems Biology, New York University, Abu Dhabi, UAE; (4) Cellular and Synaptic Physiology, National Institute of Child Health and Human Development, NIH, Bethesda, MD, USA; (5) Surgical Neurology, National Institute of Neurological Disorders and Stroke, NIH, Bethesda, MD, USA; (6) McGovern Institute for Brain Research, Massachusetts Institute of Technology, Cambridge, MA, USA; (7) Systems Neurobiology Laboratories, The Salk Institute for Biological Studies, La Jolla, CA, USA; (8) Comprehensive Epilepsy Center, New York University School of Medicine, New York, NY, USA; (9) Department of Neuroscience, Albert Einstein College of Medicine, Bronx, NY, USA; (10) Department of Neuroscience, The University of Pennsylvania Perelman School of Medicine, Philadelphia, PA

Recent success in identifying gene regulatory elements in the context of recombinant adeno-associated virus vectors have enabled cell type-restricted gene expression. However, within the cerebral cortex these tools are presently limited to broad classes of neurons. To overcome this limitation, we developed a strategy that led to the identification of multiple novel enhancers to target functionally distinct neuronal subtypes. By investigating the regulatory landscape of the disease gene *Scn1a,* we identified enhancers that target the breadth of its expression, including two selective for parvalbumin and vasoactive intestinal peptide cortical interneurons. Demonstrating the functional utility of these elements, we found that the PV-specific enhancer allowed for the selective targeting and manipulation of fast-spiking cortical interneurons across species, from mice to humans.

Sequencing studies have identified hundreds of pathogenic variants that can cause neurological and psychiatric disorders (1-5). With the advent of large-scale transcriptomic studies, we are rapidly determining where and when these genes are expressed with respect to specific cell types (6-9). Further progress will require methods for targeting and manipulating these cells. Thus, facilitating access in mice and gaining it in non-human primates and humans has become paramount. Such progress would increase our understanding of the physiological and biochemical function of specific cell types and enable targeted circuit modulation under normal and pathological conditions.

AAVs have become the method of choice for gene delivery in the nervous system but have a limited genomic payload and are not intrinsically selective for particular neuronal populations (10). We and others have identified small regulatory elements capable of restricting viral expression to broad populations. Systematic enhancer discovery depends upon identification of gene expression within specific cell types, in addition to determining chromatin accessibility and sequence conservation at these gene loci. These efforts have been made possible by the recent development of technologies allowing for transcriptomics and epigenetic studies at single-cell resolution, such as ATAC-seq, DNA-methylation sequencing (11-18). Even with these methods to refine enhancer selection, the search space remains enormous and to date success has been limited.

To focus our enhancer selection, we chose to specifically examine the regulatory landscape of *Scn1a*, a gene causing a spectrum of epilepsies expressed in distinct and non-overlapping neuronal populations in the cortex (19-24). Coupling this with chromatin accessibility data relevant to the various neuronal populations expressing this gene, we were reduced our selection of enhancers to ten elements. By thoroughly investigating each of these elements, we were identified three that covered the cell populations expressing *Scn1a.* In particular, we focused on an enhancer whose expression was restricted to parvalbumin-expressing cortical interneurons (PV cINs). To fully assess the utility of this element beyond reporter expression, we demonstrate its utility in a variety of contexts, including synaptic tagging, calcium imaging, as well as opto- and chemo-genic approaches. Moreover, this element significantly broadens our ability to target PV cINs both during development and across species including rodents, non-human primates and humans.

Our efforts led to the discovery of a variety of tools that enable understanding of the connection between a disease gene and the cell types affected in normal development and disease.

Identification of Scn1a enhancers

Scn1a encodes for Nav1.1, a sodium channel expressed three non-overlapping neuronal populations, including fast-spiking cortical interneurons expressing parvalbumin (PV cINs), dis-inhibitory cortical interneurons expressing the vaso-intestinal peptide (VIP cINs) and layer 5 pyramidal neurons (19, 25, 26). Haploinsufficiency or critical pathogenic missense mutations of *Scn1a* cause Dravet Syndrome, a common and intractable form of epileptic encephalopathy characterized by an early onset of seizure (19-26). As a starting point for devising a genetic strategy to target the distinct cortical populations expressing this gene, we developed an integrative method to systematically identify candidate enhancers within this locus. Ten putative enhancers were selected (E1 to E10) based on the following assumptions (figure 1A). First, it has been suggested that the closer an enhancer is to its transcriptional start site (TSS), the stronger the level of gene expression attained (27). Hence, to maximize our chances to identify enhancers capable of driving functional levels of transgenes, we examined the intergenic and intronic regions of Scn1a closest to its TSS. Second, the location of active enhancers within a given cell type correlates with chromatin accessibility and DNA hypomethylation. Using bulk ATAC-seq profiling (28) and single-nucleus-MethylC-seq data (29), we identified chromatin regions accessible in PV cINs, VIP cINs and pyramidal neurons. These represent the three cortical neuron populations that express the highest levels of Scn1a. Third, since functional enhancers are conserved across species (28-34), we focused on those sequences showing the highest conservation across mammalian species, including humans (see method section). Aiming to identify enhancers with therapeutic potential, we sought chromatic accessible intronic regions near TSS that are highly conserved through evolution as candidates.

To examine the ability of the candidate enhancers to target populations that express Scn1a, they were inserted into an rAAV-backbone containing a minimal promoter upstream of a red fluorescent reporter (rAAV-E[x]-dTomato). From these constructs, rAAVs were then produced with the PHPeB capsid and subsequently systemically administered into adult mice (35, 36). After 3 weeks, all viruses showed strong and sparse expression within the cortex, as well as across multiple brain regions (supplementary figures 1). Except for E5, the vast majority of virally-labelled cells expressed the interneuron marker Gad1. However, the degree of co-localization for PV within cortical neurons varied, ranging from over 90% for E2 to below 5% for E6, with all remaining enhancers displaying an intermediate level of PV expression (figure 1B). Next, we further

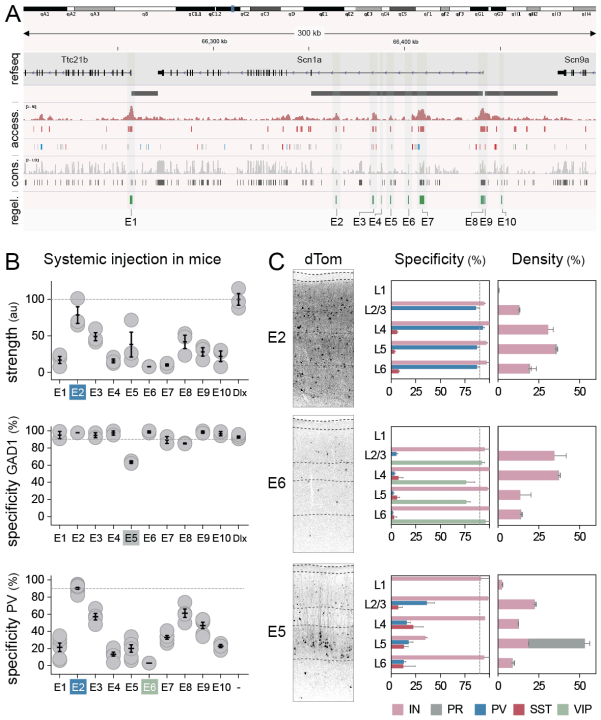

Figure 1. Identification of Scn1a enhancers. (A) Schematic representation of the enhancer selection method. See method section for complete description. (**B, C)** Adult mice were injected systemically with rAAVs expressing the reporter dTomato under the control of the indicated regulatory element and analyzed 4 weeks post-injection. The strength of expression of the reporter (B - upper panel) or the specificity of expression of the viral reporter for the indicated markers (B - lower panels) was assessed by immunohistochemistry in the somatosensory cortex. (**C**) The specificity of expression is reported as the proportion of virally labeled cells that co-express the indicated marker gene in the indicated cortical layer. Dashed lines represent the limits of anatomical structures. Scale bars represent 100um. On the graphs, the dots represent individual measurements and the lines represent average +/- s.e.m. (see supplementary table 1 for values and n).

examined the identity and layer distribution of the neuronal populations captured by the E2, E6 and E5 enhancers. Consistent with their layer distribution, co-localization analysis with various markers revealed that the E2 regulatory element restricted the expression of the viral reporter to PV cINs, while E6 was selective for VIP interneurons (Figure 1Cii). By contrast, the E5 regulatory element, while sparsely labeling interneuron populations across all layers, had a notable enrichment for pyramidal neurons in layer 5 (figure 1C). These data indicate that a significant fraction of the cortical expression profile of Scn1a in the cortex is cumulatively mirrored by the collective expression of these 3 enhancers. Importantly, these regulatory elements are responsible for largely non-overlapping expression in populations of neurons with distinct functions and developmental origins. These viruses thus provide a means of dissecting the contribution of different neuronal populations to normal and diseased cortex.

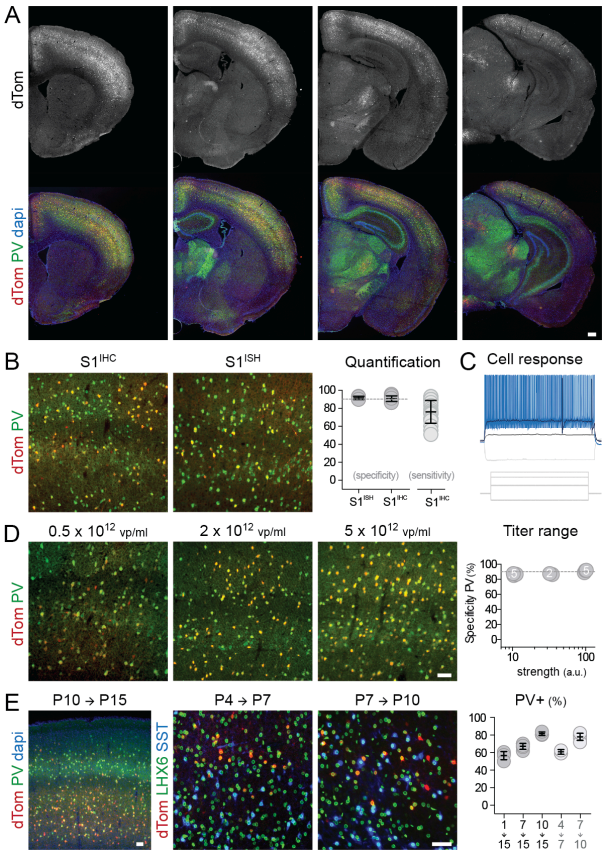

Figure 2. Viral targeting of PV cINs in mice. Adult mice were injected systemically **(A-C)** or locally **(D)** with rAAVs expressing the reporter dTomato under the control of the E2 regulatory element and analyzed 4 weeks post-injection by immuno-histochemistry for the reporter and the indicated markers. **(C)** Slice recoding of the intrinsic properties of virally labeled neurons. **(D - right panel)**. The specificity of expression is shown as the proportion of cells expressing the reporter that co-express the PV relative to the strength of expression of the reporter. **(E)** Mice were injected locally with rAAVs expressing the reporter dTomato under the control of the E2 regulatory element and analyzed at the indicated developmental stages for the reporter and the indicated markers. Scale bars represent 250um (A) and 50um (B, D, E). On the graphs, the dots represent individual measurements and the lines represent average +/- s.e.m. (see supplementary table 1 for values and n).

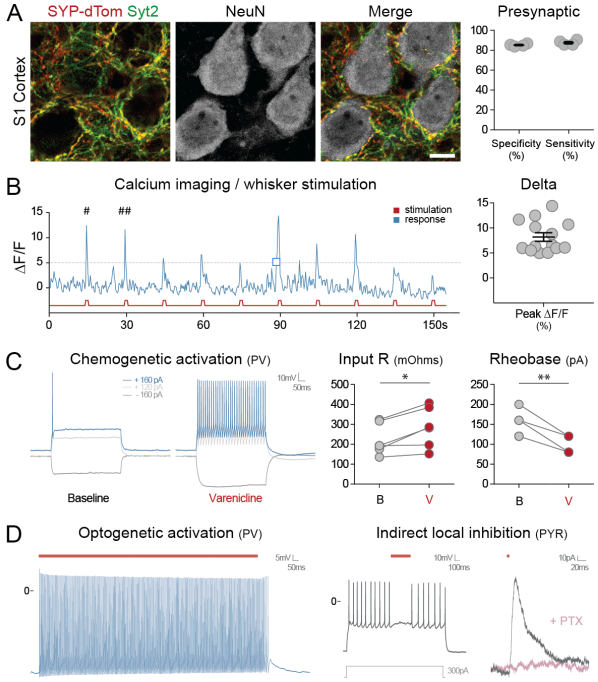

Figure 3. Viral monitoring and manipulation of PV cINs in mice. Mice were injected locally in the somatosensory cortex with rAAVs (**A** – P10 injection with rAAV-E2-SYP-dTomato; **B** – P14 injections with rAAV-E2-GCaMP6f; **C** – Adult injection with rAAV-E2-C1V1-eYFP) and systemically with rAAVs (**D** – Adult injection with rAAV-E2-PSAM4-5HT3-LC-GFP). (**A**) Mice were analyzed one-week post-injection. The specificity of expression is shown as the proportion of virally labeled presynaptic puncta co-expressing the PV synaptic marker Syt2. The sensitivity of expression is shown as the proportion of Syt2+ synapses co-expressing the viral synaptic reporter. (**B**) Ca2+ imaging with whisker stimulation was done 2-3 weeks after injection. (**C**) Slice electrophysiology current clamp recordings were performed 4 weeks after injection. The traces show a representative cellular response at the indicated currents, both at baseline and upon bath application of varenicline (5min). (**D**) Slice electrophysiology current clamp recordings were performed 1 week after injection. Cells expressing the viral reporter were targeted and recording of voltage over 3s upon 2 seconds of constant laser stimulation (550nm) were performed. The red bars above the recording traces represent laser stimulation. *pvalue < 0.05 ** pvalue < 0.01 - Dashed lines represent the limits of anatomical structures. Scale bar represents 5um. Red bars above the traces represent whisker-, opto- or chemo-genetic stimulation. On the graphs, the dots represent individual measurements and the lines represent average +/- s.e.m. (see supplementary table 1 for values and n).

Viral targeting of PV cINs in mice

With 90% specificity for PV cINs, the E2 regulatory elements allows for the targeting of fast-spiking neurons, which collectively constitute 40% of all cortical interneurons. These neurons exert a strong level of control over local networks and their disfunction has been directly implicated in neurological and neuropsychiatric disorders including Dravet syndrome, focal epilepsy, ASD and schizophrenia (37,38). As such, gaining control over their activity is of particular interest for both fundamental research and clinical applications. Thus, we focus our efforts on the characterizing the E2 regulatory element, in order to develop a viral tool with broad utility. Adult mice systemically-injected with rAAV-E2-dTomato showed detectable expression of the viral reporter after one week, which reached a high and stable level of expression after 3 weeks. Immunohistochemistry and in situ hybridization were consistently showed that ~90% of virally labeled cells were PV cINs in the cortex. Conversely, on average 75% of PV cINs expressed the viral reporter, with a maximum sensitivity reaching 93% (figure 2A and 2B). This suggests that E2 is capable of targeting all PV cINs without bias for layers or subtypes. Consistent with the specificity, slice recordings from mice showed that the cells expressing the reporter exhibited electrophysiological properties characteristic of fast-spiking cINs (figure 2C and supplementary figure 2A). The viral reporter is predominantly confined to the cortex, but some level of expression was observed in other regions closely corresponding to areas of Scn1a expression. In these regions, E2 maintained high specificity to PV-expressing cells within V1 and cingulate

cortex, subiculum, hippocampal CA1, substantia nigra pars reticulata (supplementary figure 2B). Many experimental paradigms and clinical applications will require local rather than systemic injection. To be useful in these contexts, viral expression must retain a high level of specificity for PV cINs. Stereotactically guided injections typically lead to a higher number of viral particles per cell compared to systemic delivery, which in some contexts may result in off-target expression. To test whether increasing the viral load altered the specificity, we locally injected the same volume of rAAV-E2-dTomato at various titers into the S1 cortex of adult mice and assessed reporter expression within PV cINs after a week (figure 2D). The results show that while higher titers had increased levels of reporter expression, no significant alteration of specificity was observed.

Despite the prevalence of PV-expressing interneurons in the mature cortex, targeting them at early postnatal stages has been hampered by the relatively late expression of PV itself (~ 15 days after birth - P15). Their involvement in developmental neuropsychiatric disorders highlights the importance of targeting and manipulating this cell population during cortical circuit assembly. While complex genetic strategies offer a partial solution to achieving this in mice (i.e. Lhx6-Cre, Sst-Flp and Cre and Flp-dependent reporter), even this approach does not offer the means to easily manipulate this population before two weeks postnatally. To test whether the E2 enhancer can target fast-spiking cINs before the onset of expression of parvalbumin, we examined its activity at various postnatal stages. To this end, we tiled our analysis across the early postnatal period, through a series of stereotactically-guided injections of rAAV-E2-dTomato (figure 2E). We then assessed selectivity of the reporter upon the onset of PV expression at P15. This revealed that we could obtain above 50% selectivity for PV cells upon injection at P1, increasing to 67% by P7 injection and over 80% after P10 injection. We next wondered if we could use this approach to label PV cINs prior to P15. To identify fast spiking cINs prior to this stage, we relied on Lhx6-Cre/Intact transgenic mice, in which GFP is expressed in MGE-derived interneurons (both PV and SST). By co-staining for SST, the PV cINs can be distinguished as GFP-positive/SST-negative. We obtained 60% and 78% specificity for PV with a P4-P7 or a P7-P10 time course, respectively. Thus, our approach provides a means to study these neurons during circuit maturation using a single viral injection.

Viral monitoring and manipulation of PV cINs in mice.

Having demonstrated the fidelity of E2 expression for PV cINs with differing modes of injection and across developmental stages, we then explored the utility of this vector for studying connectivity (using a presynaptic reporter) and activity (using imaging, coupled with a genetically encoded calcium-reporter). When E2 was used to drive a synaptophysin-tdTomato fusion gene (39), reporter expression was restricted pre-synaptically to PV cINs, with terminals peri-somatically located onto pyramidal neurons (figure 3A). When this vector was used to drive GCaMP6f expression, we demonstrated that upon whisker stimulation, PV cINs were recruited (figure 3B). Together these results demonstrate that E2 provides an effective means to monitor various aspects of PV cIN biology. We next examined whether E2 was sufficient to elicit functional changes in activity (using chemo- or optogenetics). When E2 was used to direct the expression of the chemogenetic receptor PSAM4-5HT3-LC (40), we observed that PV cINs exposed to the actuator varenicline could be induced to fire when current clamped below threshold (figure 3C). Similarly, both constant and high frequency laser stimulation of PV cINs expressing the red-shifted opsin C1V1 (41) resulted in time-locked firing (figure 3D and supplementary figure 3B). Demonstrating that engagement of these neurons resulted in concomitant local inhibition, pyramidal neuron activity in the vicinity of virally labeled PV cINs was interrupted by laser stimulation, an effect abolished by treatment with picrotoxin (figure 3D). Overall, these efforts show that E2 is able to functionally engage PV cINs using chemo- or optogenetics.

Viral targeting and manipulation of PV cortical interneurons in primates including humans

The sequence of the E2 enhancer is highly conserved across mammalian species, including humans. This is suggestive of a conserved role in gene regulation. We thus sought to establish whether this element could be used to target interneurons across mammalian species. Using systemic (marmoset) or focal injections (rat and macaque) of E2 virus, we were able to target PV cINs with approximately 90% specificity (figure 4A). Recently researchers have discovered that human brain tissue obtained during surgery can be cultured for prolonged periods (42). Taking advantage of the resilience of human brain to remain healthy *ex vivo,* we exposed freshly resected subiculum or medial temporal cortex to E2 virus. Over the two-week culture period, we observed the progressive appearance of fluorescently labeled cells. In regions where PV staining was reflective of the expected distribution of these cells, virally labeled cells were PV-positive (figure 4Bi; see methods for details). In addition, the majority of cells within both the cortex and subiculum showed the characteristic hallmarks of PV basket cells as indicated by multiple criteria. These include morphology

(figure 4Bii and supplementary figure 4A), maximum firing rate when evoked through direct depolarization (figure 4Bii-iii and supplementary figure 4B) or optogenetic light stimulation (figure 4Biv). These results indicate that the E2 vector provides an effective tool for targeting and manipulating PV cINs across mammals, including humans.

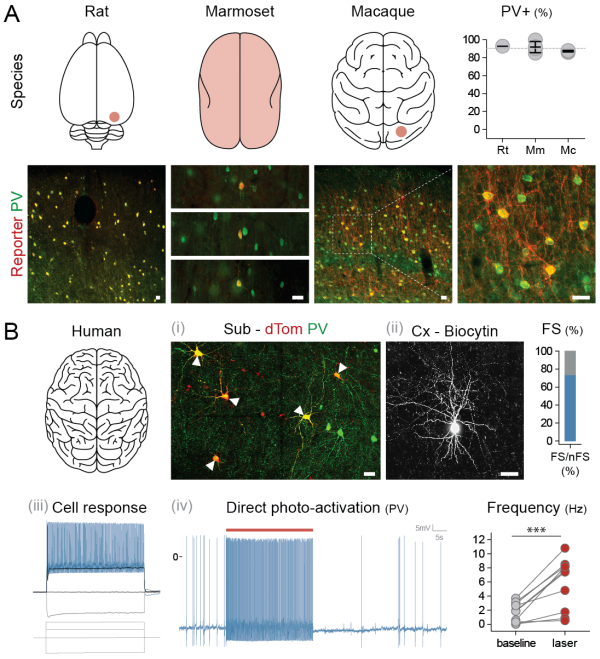

Figure 4. Viral targeting and manipulation PV cortical interneurons in primates including humans. (**A**) Animals from the indicated species were locally (rat and macaque) or systemically (marmoset) injected with AAV-E2-C1V1-eYFP (macaque) or AAV-E2-dTomato (rat and marmoset) and analyzed 2-8 weeks after the injection. The specificity of expression is shown as the proportion of virally labeled cells co-expressing PV. (**B**). Human brain tissue obtained from surgical resection was exposed to either AAV-E2-dTomato (**i,ii**) or AAV-E2-C1V1-eYFP (**iii**) and maintained in culture for 7-14 days. Scale bars represent 25um. On the graphs, the dots represent individual measurements and the lines represent average +/- s.e.m. (see supplementary table 1 for values and n). Red bars represent laser stimulation and the arrowheads point at neurons co-expressing PV and the viral reporter.

Discussion

A challenge in understanding neurological disorders stems from the complexity of the neuronal types involved. Here, in an effort to deconvolve the cellular actions of a disease gene, we systematically dissected the Scn1a locus and identified ten different enhancers distributed across the intronic and intergenic region of this gene. By creating AAVs whose expression depends on each of these enhancers, we were able to identify three that recapitulate the global pattern of *Scn1a* gene expression. The remaining seven elements were highly specific for GAD1 and labeled an assortment of interneuron subpopulations. While each of these likely recruits distinct combinations of subtypes, characterizing their possible utility is beyond the scope of this study. By contrast, the E2 enhancer was selective for a particular cIN subtype, the PV-expressing fast spiking cells. As loss of expression of *Scn1a* is especially associated with PV cIN disfunction, we focused on the E2 enhancer, which proved particularly adept at selectively targeting this population not only in rodents but also within various primates, including humans. This enhancer also proved useful for investigating aspects of PV cIN function including connectivity, monitoring excitability, and for manipulating their activity with optogenetics. The demonstration of the utility of the E2 enhancer in a range of species highlights the breadth of possible basic and clinical applications of this approach. Further potential uses include: broader exploration of circuits (e.g. creating starter cells for monosynaptic tracing using recombinant-rabies), cell type-specific gene loss of function (e.g CRISPR) and targeted drug screens. Notably, this also opens the possibility to study specie's specific differences in the numbers, distribution or physiological properties of PV cINs (43-45). If generalizable to other cell types, this approach will be transformative for investigating a range of species, most notably both primates and humans.

In this study we have taken the strategy of systematically examining enhancers at a specific disease locus, the *Scn1a* gene. Our success in identifying key regulatory elements for each of the cell types that express this gene highlights the benefits of this approach. It both clarifies the expression of this gene and simultaneous provides a toolkit to manipulate the activity of distinct subpopulations that express it. Further genes that might be candidate for similar analyses include *Mecp2, Shank3* and *Erbb4,* all of which have significant clinical importance, involving their selective expression in specific neuronal subtypes (46-48).

Many of the SNPs associated with the *Scn1a* locus map to intron 1 (49-51). The three enhancers we identified as highly specific for *Scn1a*-expressing populations were located within this region. It is tempting to speculate that the identified SNPs reflect mutations in these enhancers that affect their ability to properly direct the expression of *Scn1a*. E2 is of particular interest, as conditional removal of *Scn1a* from forebrain interneurons has been shown to recapitulate the seizure phenotype in mice. As *Scn1a* expression is largely restricted to the PV-expressing subpopulation of interneurons, mutations in the E2 enhancer may be a direct cause of Dravet syndrome.

A major impediment to examine early dynamics of circuit maturation is the inaccessibility to specific cell types without the use of transgenic animals. Young PV cINs have been particularly problematic to target even with complex genetic strategies. Given their abundance (they represent 40% of all inhibitory

cINs), as well as their implication in both the maturation of cortical circuits and neurodevelopmental disorders, gaining access to them prior to the onset of PV expression has been long awaited by the field. The unprecedented specificity of the E2 enhancer at these developmental stages and the simplicity of the viral injection over genetics provides the means to study their normal development and role in disease.

More broadly, the three enhancers identified in this study provide access to particular populations with distinct clinical relevance. Most obviously these enhancers can potentially be leveraged to alleviate debilitating aspects of Dravet syndrome, through either gene therapy or modulation of neuronal activity (52). In this manuscript, we demonstrate that local and systemic injections can be used for effective viral delivery to the brain. Both of these provide opportunities for clinical interventions. With local injections, one could possibly ameliorate focal epilepsy, prefrontal cortex dysfunction or hippocampal memory disorders. By contrast, systemic introduction of virus could be used in contexts where global interventions are necessary. For instance, to correct generalized seizures, or for psychiatric and neurodegenerative disorders. Our study shows that the rigorous identification of regulatory elements provides a road map for accessing specific cell types in both experimental and therapeutic contexts.

References

1. Rubenstein, J. L. R. & Merzenich, M. M. Model of autism: increased ratio of excitation/inhibition in key neural systems. Genes, Brain and Behavior 2, 255–267 (2003).

2. Lubeiro, A., Fatjó-Vilas, M., Guardiola, M., Almodóvar, C., Gomez-Pilar, J., Cea-Cañas, B., Poza, J., Palomino, A., Gómez-García, M., Zugasti, J. & Molina, V. Analysis of KCNH2 and CACNA1C schizophrenia risk genes on EEG functional network modulation during an auditory odd-ball task. Eur Arch Psychiatry Clin Neurosci 33, 21–10 (2019).

3. Turetsky, B. I., Dress, E. M., Braff, D. L., Calkins, M. E., Green, M. F., Greenwood, T. A., Gur, R. E., Gur, R. C., Lazzeroni, L. C., Nuechterlein, K. H., Radant, A. D., Seidman, L. J., Siever, L. J., Silverman, J. M., Sprock, J., Stone, W. S., Sugar, C. A., Swerdlow, N. R., Tsuang, D. W., Tsuang, M. T. & Light, G. The utility of P300 as a schizophrenia endophenotype and predictive biomarker: Clinical and socio-demographic modulators in COGS-2. Schizophr. Res.163, 53–62 (2015).

4. Krishnan, A., Zhang, R., Yao, V., Theesfeld, C. L., Wong, A. K., Tadych, A., Volfovsky, N., Packer, A., Lash, A. & Troyanskaya, O. G. Genome-wide prediction and functional characterization of the genetic basis of autism spectrum disorder. Nature Neuroscience 19, 1454–1462 (2016).

5. Pardiñas, A. F., Holmans, P., Pocklington, A. J., Escott-Price, V., Ripke, S., Carrera, N., Legge, S. E., Bishop, S., Cameron, D., Hamshere, M. L., Han, J., Hubbard, L., Lynham, A., Mantripragada, K., Rees, E., MacCabe, J. H., McCarroll, S. A., Baune, B. T., Breen, G., Byrne, E. M., Dannlowski, U., Eley, T. C., Hayward, C., Martin, N. G., McIntosh, A. M., Plomin, R., Porteous, D. J., Wray, N. R., Caballero, A., Geschwind, D. H., Huckins, L. M., Ruderfer, D. M., Santiago, E., Sklar, P., Stahl, E. A., Won, H., Agerbo, E., Als, T. D., Andreassen, O. A., Baekvad-Hansen, M., Mortensen, P. B., Pedersen, C. B., Borglum, A. D., Bybjerg-Grauholm, J., Djurovic, S., Durmishi, N., Pedersen, M. G., Golimbet, V., Grove, J., Hougaard, D. M., Mattheisen, M., Molden, E., Mors, O., Nordentoft, M., Pejovic-Milovancevic, M., Sigurdsson, E., Silagadze, T., Hansen, C. S., Stefansson, K., Stefansson, H., Steinberg, S., Tosato, S., Werge, T., GERAD1 Consortium:, CRESTAR Consortium:, Collier, D. A., Rujescu, D., Kirov, G., Owen, M. J., O'Donovan, M. C. & Walters, J. T. R. Common schizophrenia alleles are enriched in mutation-intolerant genes and in regions under strong background selection. Nature Genetics 50, 381–389 (2018).

6. Skene, N. G., Bryois, J., Bakken, T. E., Breen, G., Crowley, J. J., Gaspar, H. X. L. X. N. A., Giusti-Rodríguez, P., Hodge, R. D., Miller, J. A., oz-Manchado, A. B. M. X., Donovan, M. C. O. X., Owen, M. J., as, A. F. P. X., Ryge, J., Walters, J. T. R., Linnarsson, S., Lein, E. S., Sullivan, P. F. & Hjerling-Leffler, J. Genetic identification of brain cell types underlying schizophrenia. Nature Genetics 1–15 (2018). doi:10.1038/s41588-018-0129-5

7. Voineagu, I., Wang, X., Johnston, P., Lowe, J. K., Tian, Y., Horvath, S., Mill, J., Cantor, R. M., Blencowe, B. J. & Geschwind, D. H. Transcriptomic analysis of autistic brain reveals convergent molecular pathology. Nature 474, 380–384 (2011).

8. Parikshak, N. N., Luo, R., Zhang, A., Won, H., Lowe, J. K., Chandran, V., Horvath, S. & Geschwind, D. H. Integrative functional genomic analyses implicate specific molecular pathways and circuits in autism. Cell 155, 1008–1021 (2013).

9. Camp JG, Platt R, Treutlein B. Mapping human cell phenotypes to genotypes with single-cell genomics. Science. 2019 Sep 27;365(6460):1401-1405. doi: 10.1126/science.aax6648. Review PMID:31604266

10. Bedbrook CN, Deverman BE, Gradinaru V. Viral Strategies for Targeting the Central and Peripheral Nervous Systems. Annu Rev Neurosci. 2018 Jul 8;41:323-348. doi: 10.1146/annurev-neuro-080317-062048. Epub 2018 Apr 25. Review. PMID: 29709207

11. Deverman BE, Ravina BM, Bankiewicz KS, Paul SM, Sah DWY. Gene therapy for neurological disorders: progress and prospects. Nat Rev Drug Discov. 2018 Sep;17(9):641-659. doi: 10.1038/nrd.2018.110. Epub 2018 Aug 10. Review. Erratum in: Nat Rev Drug Discov. 2018 Oct;17(10):767. PMID:30093643

12. Dimidschstein J, Chen Q, Tremblay R, Rogers SL, Saldi GA, Guo L, Xu Q, Liu R, Lu C, Chu J, Grimley JS, Krostag AR, Kaykas A, Avery MC, Rashid MS, Baek M, Jacob AL, Smith GB, Wilson DE, Kosche G, Kruglikov I, Rusielewicz T, Kotak VC, Mowery TM, Anderson SA, Callaway EM, Dasen JS, Fitzpatrick D, Fossati V, Long MA, Noggle S, Reynolds JH, Sanes DH, Rudy B, Feng G, Fishell G. A viral strategy for targeting and manipulating interneurons across vertebrate species. Nat Neurosci. 2016 Dec;19(12):1743-1749. doi: 10.1038/nn.4430. Epub 2016 Oct 31. Update in: Nat Neurosci. 2017 Jun 27;20(7):1033. Erratum in: Nat Neurosci. 2017 Jun 27;20(7):1033. PMID:27798629

13. de Leeuw CN, Korecki AJ, Berry GE, Hickmott JW, Lam SL, Lengyell TC, Bonaguro RJ, Borretta LJ, Chopra V, Chou AY, D'Souza CA, Kaspieva O, Laprise S, McInerny SC, Portales-Casamar E, Swanson-Newman MI, Wong K, Yang GS, Zhou M, Jones SJ, Holt RA, Asokan A, Goldowitz D, Wasserman WW, Simpson EM. rAAV-compatible Mini-Promoters for restricted expression in the brain and eye. Mol Brain. 2016 May 10;9(1):52. doi: 10.1186/s13041-016-0232-4. PMID:27164903

14. Jüttner J, Szabo A, Gross-Scherf B, Morikawa RK, Rompani SB, Hantz P, Szikra T, Esposti F, Cowan CS, Bharioke A, Patino-Alvarez CP, Keles Ö, Kusnyerik A, Azoulay T, Hartl D, Krebs AR, Schübeler D, Hajdu RI, Lukats A, Nemeth J, Nagy ZZ, Wu KC, Wu RH, Xiang L, Fang XL, Jin ZB, Goldblum D, Hasler PW, Scholl HPN, Krol J, Roska B. Targeting neuronal and glial cell types with synthetic promoter AAVs in mice, non-human primates and humans. Nat Neurosci. 2019 Aug;22(8):1345-1356. doi: 10.1038/s41593-019-0431-2. Epub 2019 Jul 8.PMID:31285614

15. Hrvatin S, Tzeng CP, Nagy MA, Stroud H, Koutsioumpa C, Wilcox OF, Assad EG, Green J, Harvey CD, Griffith EC, Greenberg ME. A scalable platform for the development of cell-type-specific viral drivers. Elife. 2019 Sep 23;8. pii: e48089. doi: 10.7554/eLife.48089. PMID:31545165

16. Lucas T Graybuck, Adriana Sedeño-Cortés, Thuc Nghi Nguyen, Miranda Walker, Eric Szelenyi, Garreck Lenz, La'Akea Sieverts, Tae Kyung Kim, Emma Garren, Brian Kalmbach, Shenqin Yao, Marty Mortrud, John Mich, Jeff Goldy, Kimberly A Smith, Nick Dee, Zizhen Yao, Ali Cetin, Boaz P Levi, Ed Lein, Jonathan Ting, Hongkui Zeng, Tanya Daigle, Bosiljka Tasic. Prospective, brain-wide labeling of neuronal subclasses

with enhancer-driven AAVs. Preprint on Biorxiv at doi: https://doi.org/10.1101/525014

17. Rajeevkumar Raveendran Nair, Stefan Blankvoort, Maria Jose Lagartos, Cliff Kentros Generation of viral vectors specific to neuronal subtypes of targeted brain regions by Enhancer-Driven Gene Expression (EDGE) Preprint on Biorxiv at doi: https://doi.org/10.1101/606467

18. Mehta P, Kreeger L, Wylie DC, Pattadkal JJ, Lusignan T, Davis MJ, Turi GF, Li WK, Whitmire MP, Chen Y, Kajs BL, Seidemann E, Priebe NJ, Losonczy A, Zemelman BV. Functional Access to Neuron Subclasses in Rodent and Primate Forebrain. Cell Rep. 2019 Mar 5;26(10):2818-2832.e8. doi: 10.1016/j.celrep.2019.02.011. PMID: 30840900

19. Ogiwara I, Miyamoto H, Morita N, Atapour N, Mazaki E, Inoue I, Takeuchi T, Itohara S, Yanagawa Y, Obata K, Furuichi T, Hensch TK, Yamakawa K. Nav1.1 localizes to axons of parvalbumin-positive inhibitory interneurons: a circuit basis for epileptic seizures in mice carrying an Scn1a gene mutation. J Neurosci. 2007 May 30;27(22):5903-14. PMID: 17537961

20. Griffin A, Hamling KR, Hong S, Anvar M, Lee LP, Baraban SC. Preclinical Animal Models for Dravet Syndrome: Seizure Phenotypes, Comorbidities and Drug Screening. Front Pharmacol. 2018 Jun 4;9:573. doi: 10.3389/fphar.2018.00573. eCollection 2018. Review. PMID: 29915537

21. Cheah CS, Yu FH, Westenbroek RE, Kalume FK , Oakley JC, Potter GB, Rubenstein JL, Catterall WA. Specific deletion of Nav1.1 sodium channels in inhibitory interneurons causes seizures and premature death in a mouse model of Dravet Syndrome. PNAS. 2012 Sep 4;109(36):14646-51. PMID: 22908258

22. Yu FH, Mantegazza M, Westenbroek RE, Robbins CA, Kalume F, Burton KA, Spain WJ, McKnight GS, Scheuer T, Catterall WA. Reduced sodium current in GABAergic interneurons in a mouse model of severe myoclonic epilepsy in infancy. Nature Neuroscience. 2006 Sep;9(9):1142-9 Epub 2006 Aug 20. PMID: 16921370

23. Kalume F, Westenbroek RE, Cheah CS, Yu FH, Oakley JC, Scheuer T, Catterall WA. Sudden unexpected death in a mouse model of Dravet syndrome. J Clin Invest. 2013 Apr;123(4):1798-808. doi: 10.1172/JCI66220. Epub 2013 Mar 25. PMID:23524966

24. Papale LA, Makinson CD, Christopher Ehlen J, Tufik S, Decker MJ, Paul KN, Escayg A. Altered sleep regulation in a mouse model of SCN1A-derived genetic epilepsy with febrile seizures plus (GEFS+). Epilepsia. 2013 Apr;54(4):625-34. doi: 10.1111/epi.12060. Epub 2013 Jan 11. PMID: 23311867

25. Favero M, Sotuyo NP, Lopez E, Kearney JA, Goldberg EM. A Transient Developmental Window of Fast-Spiking Interneuron Dysfunction in a Mouse Model of Dravet Syndrome. J Neurosci. 2018 Sep 5;38(36):7912-7927. doi: 10.1523/JNEUROSCI.0193-18.2018. Epub 2018 Aug 13. PMID: 30104343

26. Goff KM, Goldberg EM. Vasoactive intestinal peptide-expressing interneurons are impaired in a mouse model of Dravet syndrome. Elife. 2019 Jul 8;8. pii: e46846. doi: 10.7554/eLife.46846. PMID:31282864

27. Fulco CP, Munschauer M, Anyoha R, Munson G, Grossman SR, Perez EM, Kane M, Cleary B, Lander ES, Engreitz JM. Systematic mapping of functional enhancer-promoter connections with CRISPR interference. Science. 2016 Nov 11;354(6313):769-773. Epub 2016

28. Mo, A., Mukamel, E. A., Davis, F. P., Luo, C., Henry, G. L., Picard, S., Urich, M. A., Nery, J. R., Sejnowski, T. J., Lister, R., Eddy, S. R., Ecker, J. R. & Nathans, J. Epigenomic Signatures of Neuronal Diversity in the Mammalian Brain. Neuron 86, 1369–1384 (2015).

29. Luo C, Rivkin A, Zhou J, Sandoval JP, Kurihara L, Lucero J, Castanon R, Nery JR, Pinto-Duarte A, Bui B, Fitzpatrick C, O'Connor C, Ruga S, Van Eden ME, Davis DA, Mash DC, Behrens MM, Ecker JR. Robust single-cell DNA methylome profiling with snmC-seq2. Nat Commun. 2018 Sep 20;9(1):3824. doi: 10.1038/s41467-018-06355-2. PMID:30237449

30. Dousse A, Junier T, Zdobnov EM. CEGA--a catalog of conserved elements from genomic alignments. Nucleic Acids Res. 2016 Jan 4;44(D1):D96-100. doi: 10.1093/nar/gkv1163. Epub 2015 Nov 2. PMID: 26527719

31. Bejerano G, Pheasant M, Makunin I, Stephen S, Kent WJ, Mattick JS, Haussler D. Ultraconserved elements in the human genome. Science. 2004 May 28;304(5675):1321-5. Epub 2004 May 6.

32. Dickel DE, Ypsilanti AR, Pla R, Zhu Y, Barozzi I, Mannion BJ, Khin YS, Fukuda-Yuzawa Y, Plajzer-Frick I, Pickle CS, Lee EA, Harrington AN, Pham QT, Garvin TH, Kato M, Osterwalder M, Akiyama JA, Afzal V, Rubenstein JLR, Pennacchio LA, Visel A. Ultraconserved Enhancers Are Required for Normal Development. Cell. 2018

33. Dimitrieva S, Bucher P. UCNEbase--a database of ultraconserved non-coding elements and genomic regulatory blocks. Nucleic Acids Res. 2013 Jan;41(Database issue):D101-9. doi: 10.1093/nar/gks1092. Epub 2012 Nov 27. PMID:23193254

34. Andersson R, Gebhard C, Miguel-Escalada I, Hoof I, Bornholdt J, Boyd M, Chen Y, Zhao X, Schmidl C, Suzuki T, Ntini E, Arner E, Valen E, Li K, Schwarzfischer L, Glatz D, Raithel J, Lilje B, Rapin N, Bagger FO, Jørgensen M, Andersen PR, Bertin N, Rackham O, Burroughs AM, Baillie JK, Ishizu Y, Shimizu Y, Furuhata E, Maeda S, Negishi Y, Mungall CJ, Meehan TF, Lassmann T, Itoh M, Kawaji H, Kondo N, Kawai J, Lennartsson A, Daub CO, Heutink P, Hume DA, Jensen TH, Suzuki H, Hayashizaki Y, Müller F, Forrest ARR, Carninci P, Rehli M, Sandelin A. An atlas of active enhancers across human cell types and tissues. Nature. 2014 Mar 27;507(7493):455-461. doi: 10.1038/nature12787. PMID:24670763

35. Deverman BE, Pravdo PL, Simpson BP, Kumar SR, Chan KY, Banerjee A, Wu WL, Yang B, Huber N, Pasca SP, Gradinaru V. Cre-dependent selection yields AAV variants for widespread gene transfer to the adult brain. Nat Biotechnol. 2016 Feb;34(2):204-9. doi: 10.1038/nbt.3440. Epub 2016 Feb 1.

36. Chan, K. Y., Jang, M. J., Yoo, B. B., Greenbaum, A., Ravi, N., Wu, W.-L., Sánchez-Guardado, L., Lois, C., Mazmanian, S. K., Deverman, B. E. & Gradinaru, V. Engineered AAVs for efficient noninvasive gene delivery to the central and peripheral nervous systems. Nature Neuroscience 20, 1172–1179 (2017).

37. Batista-Brito, R., Rossignol, E., Hjerling-Leffler, J., Denaxa, M., Wegner, M., Lefebvre, V., Pachnis, V. & Fishell, G. The Cell-Intrinsic Requirement of Sox6 for Cortical Interneuron Development. Neuron 63, 466–481 (2009).

38. Rossignol, E., Kruglikov, I., van den Maagdenberg, A. M. J. M., Rudy, B. & Fishell, G. CaV2.1 ablation in cortical interneurons selectively impairs fast-spiking basket cells and causes generalized seizures. Ann. Neurol. 74, 209–222 (2013).

39. Madisen L, Mao T, Koch H, Zhuo JM, Berenyi A, Fujisawa S, Hsu YW, Garcia AJ 3rd, Gu X, Zanella S, Kidney J, Gu H, Mao Y, Hooks BM, Boyden ES, Buzsáki G, Ramirez JM, Jones AR, Svoboda K, Han X, Turner EE, Zeng H. A toolbox of Cre-dependent optogenetic transgenic mice for light-induced activation and silencing. Nat Neurosci. 2012 Mar 25;15(5):793-802. doi: 10.1038/nn.3078. PMID:22446880

40. Magnus CJ, Lee PH, Bonaventura J, Zemla R, Gomez JL, Ramirez MH, Hu X, Galvan A, Basu J, Michaelides M, Sternson SM. Ultrapotent chemogenetics for research and potential clinical applications. Science. 2019 Apr 12;364(6436). pii: eaav5282. doi: 10.1126/science. aav5282. Epub 2019 Mar 14. PMID:30872534

41. Yizhar O, Fenno LE, Prigge M, Schneider F, Davidson TJ, O'Shea DJ, Sohal VS, Goshen I, Finkelstein J, Paz JT, Stehfest K, Fudim R, Ramakrishnan C, Huguenard JR, Hegemann P, Deisseroth K. Neocortical excitation/inhibition balance in information processing and social dysfunction. Nature. 2011 Jul 27;477(7363):171-8. doi: 10.1038/nature10360. PMID:21796121

42. Eugène E, Cluzeaud F, Cifuentes-Diaz C, Fricker D, Le Duigou C, Clemenceau S, Baulac M, Poncer JC, Miles R. An organotypic brain slice preparation from adult patients with temporal lobe epilepsy. J Neurosci Methods. 2014 Sep 30;235:234-44. doi: 10.1016/j.jneumeth.2014.07.009. Epub 2014 Jul 23. PMID: 25064188

43. Hodge RD, Bakken TE, Miller JA, Smith KA, Barkan ER, Graybuck LT, Close JL, Long B, Johansen N, Penn O, Yao Z, Eggermont J, Höllt T, Levi BP, Shehata SI, Aevermann B, Beller A, Bertagnolli D, Brouner K, Casper T, Cobbs C, Dalley R, Dee N, Ding SL, Ellenbogen RG, Fong O,

Garren E, Goldy J, Gwinn RP, Hirschstein D, Keene CD, Keshk M, Ko AL, Lathia K, Mahfouz A, Maltzer Z, McGraw M, Nguyen TN, Nyhus J, Ojemann JG, Oldre A, Parry S, Reynolds S, Rimorin C, Shapovalova NV, Somasundaram S, Szafer A, Thomsen ER, Tieu M, Quon G, Scheuermann RH, Yuste R, Sunkin SM, Lelieveldt B, Feng D, Ng L, Bernard A, Hawrylycz M, Phillips JW, Tasic B, Zeng H, Jones AR, Koch C, Lein ES. Conserved cell types with divergent features in human versus mouse cortex. Nature. 2019 Sep;573(7772):61-68. doi: 10.1038/s41586-019-1506-7. Epub 2019 Aug 21. PMID: 31435019

44. Boldog E, Bakken TE, Hodge RD, Novotny M, Aevermann BD, Baka J, Bordé S, Close JL, Diez-Fuertes F, Ding SL, Faragó N, Kocsis ÁK, Kovács B, Maltzer Z, McCorrison JM, Miller JA, Molnár G, Oláh G, Ozsvár A, Rózsa M, Shehata SI, Smith KA, Sunkin SM, Tran DN, Venepally P, Wall A, Puskás LG, Barzó P, Steemers FJ, Schork NJ, Scheuermann RH, Lasken RS, Lein ES, Tamás G. Transcriptomic and morphophysiological evidence for a specialized human cortical GABAergic cell type. Nat Neurosci. 2018 Sep;21(9):1185-1195. doi: 10.1038/s41593-018-0205-2. Epub 2018 Aug 27. PMID:30150662

45. Fenna M. Krienen, Melissa Goldman, Qiangge Zhang, Ricardo del Rosario, Marta Florio, Robert Machold, Arpiar Saunders, Kirsten Levandowski, Heather Zaniewski, Benjamin Schuman, Carolyn Wu, AlyssaLutservitz, Christopher D. Mullally, Nora Reed, Elizabeth Bien, Laura Bortolin, Marian Fernandez-Otero, Jessica Lin, Alec Wysoker, James Nemesh, David Kulp, Monika Burns, Victor Tkachev, Richard Smith, Christopher, A. Walsh, Jordane Dimidschstein, Bernardo Rudy, Leslie Kean, Sabina Berretta, Gord Fishell, Guoping Feng, Steven A. McCarroll. Innovations in Primate Interneuron Repertoire. Preprint on bioRxiv at https://doi.org/10.1101/709501

46. Chin EWM, Goh ELK. MeCP2 Dysfunction in Rett Syndrome and Neuropsychiatric Disorders. Methods Mol Biol. 2019;2011:573-591. doi: 10.1007/978-1-4939-9554-7_33. PMID:31273722

47. Monteiro P, Feng G. SHANK proteins: roles at the synapse and in autism spectrum disorder. Nat Rev Neurosci. 2017 Mar;18(3):147-157. doi: 10.1038/nrn.2016.183. Epub 2017 Feb 9. Review. PMID: 28179641

48. Rico B, Marín O. Neuregulin signaling, cortical circuitry development and schizophrenia. Curr Opin Genet Dev. 2011 Jun;21(3):262-70. doi: 10.1016/j.gde.2010.12.010. Epub 2011 Feb 4. Review. PMID: 21295966

49. Feenstra B, Pasternak B, Geller F, Carstensen L, Wang T, Huang F, Eitson JL, Hollegaard MV, Svanström H, Vestergaard M, Hougaard DM, Schoggins JW, Jan LY, Melbye M, Hviid A. Common variants associated with general and MMR vaccine-related febrile seizures. Nat Genet. 2014 Dec;46(12):1274-82. doi: 10.1038/ng.3129. Epub 2014 Oct 26. PMID:25344690

50. International League Against Epilepsy Consortium on Complex Epilepsies. Genetic determinants of common epilepsies: a meta-analysis of genome-wide association studies. Lancet Neurol. 2014 Sep;13(9):893-903. doi: 10.1016/S1474-4422(14)70171-1. Epub 2014 Jul 30. PMID:25087078

51. Genome-wide megaanalysis identifies 16 loci and highlights diverse biological mechanisms in the common epilepsies. International League Against Epilepsy Consortium on Complex Epilepsies. Nat Commun. 2018 Dec 10;9(1):5269. doi: 10.1038/s41467-018-07524-z. PMID: 30531953

52. Walker MC, Kullmann DM. Optogenetic and chemogenetic therapies for epilepsy. Neuropharmacology. 2019 Sep 5:107751. doi: 10.1016/j.neuropharm.2019.107751. [Epub ahead of print] Review. PMID: 31494141

53. Zhang, Y., Liu, T., Meyer, C. A., Eeckhoute, J., Johnson, D. S., Bernstein, B. E., Nusbaum, C., Myers, R. M., Brown, M., Li, W. & Liu, X. S. Model-based analysis of ChIP-Seq (MACS). Genome Biology 9, R137 (2008)

Methods

Animals. Mice. Female C57BL/6J mice (Mus musculus; 10 weeks old) were obtained from Jackson Labs (Bar Harbor, ME - stock# 000664). Rat. Sprague Dawley rats (adult 150-- 250 gm) were obtained from Charles River labs, Kingston, NY. Marmosets. One female common marmoset (Callithrix jacchus, 6.0 years old) was obtained from the colony at Massachusetts Institute of Technology. Macaques. One male macaque (Macaca mulatta; 15.0 years old) was obtained from the California National Primate Research Center at the University of California, Davis. All the animals were maintained in a 12 light/12 dark cycle with a maximum of five animals per cage for mice and one animal per rats. Marmosets and macaques were socially housed. All animal maintenance and experimental procedures were performed according to the guidelines established by the Institutional Animal Care and Use Committee at the Broad Institute of MIT and Harvard (mice), McGovern research institute at MIT (rats and marmosets) and Salk Institute for Biological studies (Macaques).

Enhancer selection. Selection. Candidate regulatory elements were manually curated from a list of elements generated by intersecting the "context" region (Scn1a intergenic region + intron1) with both the "ATACseq peak union" file and the "Phastcons 60-way" file – see below. Accessibility. ATAC-seq data from the Mo et al. 2015 publication were downloaded from the GEO repository and discretized as peaks using MACS2 (https://github.com/taoliu/MACS). Using a custom R script, a file containing the union of all peaks across datasets was generated and used for enhancer selection as described below. Note that the final selection relied on the inspection of the peaks for individual cell-types rather than on the union of all peaks. Methylation. Mouse mCH levels for non-overlapping 100kb bins across the entire genome for mouse from the Luo et al. 2017 publication were downloaded from Brainome portal (http://brainome.org). These data were used as a confirmation for the positioning of the candidates selected using the ATAC-seq dataset described above. Conservation. The "phascons 60-way" track was downloaded from the UCSC portal (https://genome.ucsc.edu) in BED file format and filtered using a custom R script to remove any element smaller than 10bp and fuse any element separated by less than 50bp using Bedtools/Intersect.

rAAV cloning and production. The enhancer sequences were amplified by PCR from mouse genomic DNA using the following primers: E1: caaagtggacagaggggagg and gtgctgttgggagtggtgga (1280 bp); E2: aatctaacatggctgctata and caattgctcagagttatttt (618 bp); E3: ataaaatttttattttcctaa and gaggaaatcagctacggggc (832 bp); E4: tctgacagagcaagtcttga and tatcaaaattgtatattcag (261 bp); E5: aatgttttgatatttaggag and ttgactcttaaaatttaata (663 bp); E6: ttgtcactttgttactctac and ttaaatcttaaaattttcct (606 bp); E7: gatactgtataattaattag and cttccttctggttcctttt (2430 bp); E8: attgatctccaacttttaa and gttcatccaagtaataagag (1644 bp); E9: atctcaagtgtatgtaacat and gtctttttgttttttttttt (521 bp); E10: tattgcaaaaggaaggaatg and tcatggaaaaagaaaaaatc (547 bp). The enhancers, reporters and effectors were cloned using the Gibson Cloning Assembly Kit (NEB-E5510S) following standard procedures. Specifically, for AAV-E1:10-dTomato, we amplified the dTomato coding sequence from the plasmid Addgene # 83897; for AAV-E2-SYP-dTomato, we amplified the Synaptophysin-tdTomato coding sequence from the plasmid Addgene # 34881; for AAV-E2-GCaMP6f, we amplified the GCaMP6f coding sequence from the plasmid Addgene # 83899; for AAV-E2-C1V1-eYFP, we amplified the C1V1-eYFP coding sequence from the plasmid Addgene # 35499. The rAAVs were produced using standard production methods. PEI was used for transfection and OptiPrep gradient (Sigma, USA) was used for viral particle purification. Serotype 1 was used to produce the AAVs for local injections in mice and rats. Serotype 9 was used for systemic injection in marmosets and serotype PHPeB was used for both local injection in macaques and systemic injections in mice. Titer was estimated by qPCR with primers for the WPRE sequence that is common to all constructs. All batches produced were in the range of 1010 to 1012 viral genomes per ml.

Local and systemic viral injections. Mouse local S1. Local injection in adult mice were performed by stereotactically guided injections in the somatosensory cortex with the following

coordinates 1.0 mm posterior, 2.9 mm lateral, 0.7/0.45 mm ventral relative to Bregma with 150nL of virus. Mouse systemic. For systemic injection in adult mice, approximately 10E+11 viral particles were injected in the retro-orbital sinus per animal. Post-operative monitoring was performed for five days post injection. Rat local in V1. Local injection in adult rats were performed by stereotactically guided injections in the primary visual cortex with the following coordinates 5.4 mm posterior, 4.2 mm lateral, 2.0 mm ventral relative to bregma with 670nL of virus. Marmoset systemic injection. For systemic injection in adult marmosets, approximately 10E+12 viral particles in ~ 0.7 ml of sterile PBS were injected into the saphenous vein, followed by another infusion with ~ 0.5 ml of saline. After the final infusion, pressure was applied to the injection site to ensure hemostasis. The animal was returned to its home cage and monitored closely for normal behavior post anesthesia. The animal was euthanized 51 days after viral injection. Macaque local in V1. Local injection in an adult macaque was performed by a stereotactically guided injection in the left primary visual cortex with the following coordinates: 13 mm posterior, 19 mm lateral, 23 mm superior relative to the center of the inter-aural line (based on the animal's MRI). A total of volume of 1332nL was injected, equally divided in 4 depths (i.e. 1.8, 1.3, 0.8 and 0.3 mm from the cortical surface).

Electrophysiological recordings in mice. *Slice preparation for 2 to 6-weeks-old mice.* Virally injected mice were anesthetized with isofluorane. Upon loss of reflexes, mice were transcardially perfused with ice-cold oxygenated ACSF containing the following (in mM): 87 NaCl, 75 sucrose, 2.5 KCl, 1.25 NaH_2PO_4, 26 $NaHCO_3$, 10 glucose, 1 $CaCl_2$ and 2 $MgCl_2$. Mice were then decapitated and 300-µm thick coronal slices were sectioned using a Leica VT-1200-S vibratome and incubated in a holding chamber at 32–35 °C for 15–30 min followed by continued incubation at room temperature 20–23.5 °C (68–74 °F) for at least 45–60 min before physiological recordings. Slice containing the injection site were transferred in a recording chamber submerged with oxygenated ACSF containing the following (in mM): 125 NaCl, 2.5 KCl, 1.25 NaH_2PO_4, 26 $NaHCO_3$, 10 glucose, 2 $CaCl_2$ and 1 $MgCl_2$ (pH = 7.4, bubbled with 95% O_2 and 5% CO_2). *Slice preparation for 6-weeks-old and older mice.* Acute coronal brain slices were prepared as follows. Mice were anesthetized with Avertin solution (20 mg/ml, 0.5 mg/g body weight) and transcardially perfused with 15 to 20 ml of ice-cold carbogenated (95% O_2, 5% CO_2) cutting solution containing the following: 194 mM sucrose, 30 mM NaCl, 4.5 mM KCl, 1.2 mM NaH_2PO_4, 0.2 mM $CaCl_2$, 2 mM $MgCl_2$, 26 mM $NaHCO_3$, and 10 mM D-(+)-glucose (with osmolarity of 340–350 mOsm). The brains were then rapidly removed and placed in ice-cold cutting solution for slice preparation. Coronal slices (300 µm) were prepared and then incubated at 32°C with carbogenated artificial cerebral spinal fluid (aCSF) for 10 to 15 minutes. The slices were then incubated at room temperature for at least 1 hour in aCSF that contained the following: 119 mM NaCl, 2.3 mM KCl, 1.0 mM NaH_2PO_4, 26 mM $NaHCO_3$, 11 mM glucose, 1.3 mM $MgSO_4$, and 2.5 mM $CaCl_2$ (pH 7.4, with osmolarity of 295–305 mOsm) at room temperature for at least 1 hour. Current clamp. For interneuron recording, 10 µM CNQX, 25 µM AP-5 and 10 µM SR-95531 were also added to block AMPA, NMDA and GABA-A receptors, respectively, to measure the cell-intrinsic effect of optogenetic and chemogenetic stimulation. Whole-cell current-clamp recordings were obtained from visually identified cells expressing the viral reporter using borosilicate pipettes (3–5 MΩ) containing (in mM): 130 K-gluconate, 6.3 KCl, 0.5 EGTA, 10 HEPES, 4 Mg-ATP, 0.3 Na-GTP and 0.3% biocytin (pH adjusted to 7.3 with KOH). Upon break-in, series resistance (typically 15–25 MΩ) was compensated and only stable recordings (<20% change) were included. Data were acquired using a MultiClamp 700B amplifier (Molecular Devices), sampled at 20 kHz and filtered at 10 kHz. All cells were held at −60 mV with a DC current, and current-step protocols were applied to obtain firing patterns and to extract basic sub-threshold and supra-threshold electro-physiological properties. Voltage clamp. Cells not expressing the viral reporter were selected according to their pyramidal-cell-shaped soma under IR-DIC visualization and recorded with pipettes containing (in mM): 130 Cs-gluconate, 0.5 EGTA, 7 KCl, 10 HEPES, 4 Mg-ATP, 0.3 Na-GTP, 5 phosphocreatine, 5 QX-314 and 0.3% biocytin (pH adjusted to 7.3 with CsOH). Cells were held continuously at 0 mV for baseline and optogenetic or chemogenetic stimulation. For both current and voltage clamp recording, a baseline of at least 2 min was recorded before stimulation. Small pulses (−20 pA or −5 mV, 100 ms at 0.2 Hz or 0.5 Hz) were applied throughout the baseline and CNO application to monitor series resistance changes. Data were analyzed offline using Clampfit 10.2 software (Molecular Devises).

In-vivo calcium imaging. Approximately 100 nL of AAV-E2-GCaMP6 virus was injected in barrel cortex at postnatal day 10. At P27-P34, craniotomies were implanted over the injection site and widefield calcium imaging performed after recovery from craniotomy procedure. Briefly, anesthetized (1.5% isoflurane) mice were imaged at 3-4Hz with 4x magnification (Thorlabs CCD camera – 1501M-USB, Thorlabs LED stimulation – DC4104), while air puffs (100-200ms duration, Picospritzer III) at specific intervals (5-20s) were directed at contralateral whiskers. Multiple recordings were performed and afterward the mouse was perfused for histological analysis. Recordings were analyzed in ImageJ by calculating the F/F (change in fluorescence/average fluorescence) for each recording and synched whisker stimulation. A threshold of (5%) F/F was set for both stimulated and spontaneous calcium signal response.

Electrophysiological recordings in human. *Tissue preparation*, *culture protocol and inoculation of virus.* Four participants (2 male / 2 female; age range 22-57 years) underwent a surgical procedure in which brain tissue (temporal lobe and hippocampus) was resected for the treatment of drug resistant epilepsy. In all cases, each participant had previously undergone an initial surgery for placement of subdural and/or depth electrodes for intracranial monitoring in order to identify the location of seizure onset. The NINDS Institutional Review Board (IRB) approved the research protocol (ClinicalTrials.gov Identifier NCT01273129), and we obtained informed consent from the participants for experimental use of the resected tissue. 300 um slices from both hippocampus and temporal lobe were attained (Leica 1200S Vibratome; Leica Microsystems, Bannockburn, IL) in ice-cold oxygenated sucrose based cutting solution (100mM sucrose, 80mM NaCl, 3.5mM KCl, 24mM $NaHCO_3$, 1.25mM NaH_2PO_4, 4.5mM $MgCl_2$, 0.5mM $CaCl_2$, and 10mM glucose, saturated with 95% O_2 and 5% CO_2) within 30 minutes following neurosurgical resection. Slices were then incubated in the sucrose cutting solution at 33oC for 30 minutes and allowed to cool to room temperature for 15-30 minutes. The slices were transferred to culture media (Eugène et al., 2014) and placed in an incubator (5% CO_2) at 35oC for 15 minutes of equilibration. Each individual slice was then transferred onto a 30 mm Millicell Cell Culture Insert (Millipore; Cat No. PICM0RG50) for interface culture and incubated as above. After 12 hours, the culture medium was changed and 1-2 ul of pAAV-S5E2-dTomato with or without pAAV-S5E2-C1V1-eYFP was directly pipetted onto each slice and placed back into the incubator. For hippocampal slices, the virus was targeted to the subiculum subfield. Culture medium was routinely changed every 2-3 days until electro-physiological analyses. Electro-physiological recordings. Electrophysiological recordings from cultured human slices were performed between 7 to 14 days after viral inoculation. Cultured human slices were transferred to a recording chamber perfused with extracellular solution (130 mM NaCl, 3.5 mM KCl, 24 mM $NaHCO_3$, 1.25 mM NaH_2PO_4-H_2O, 10 mM glucose, 2.5 mM $CaCl_2$ and 1.5 mM $MgCl_2$ saturated with 95% O_2/5% CO_2 (pH 7.4; 300-310 mOsm) at a

rate of 3 - 4 ml/min at 33oC. Whole cell patch clamp recordings from pAAV_S5E2-dTomato or pAAV-S5E2-C1V1-eYFP infected neurons were performed with an intracellular solution of the following composition: 130 mM K-gluconate, 10 mM HEPES, 0.6 mM EGTA, 2 mM MgCl2, 2 mM Na2ATP, 0.3 mM NaGTP and 0.5% biocytin (pH adjusted to 7.4; osmolarity adjusted to 285 - 300 mOsm). In some recordings, 130mM K-gluconate was replaced by 90 mM K-gluconate/40 KCl. Intrinsic membrane and firing properties were assayed essentially as described previously. 550nm light stimulated optogenetic activation of C1V1 was delivered to the slices via the 40X water immersion objective using a CoolLED pE-4000 Illumination system (Andover, UK). Biocytin reconstruction and immune-cytochemistry. After electrophysiological recording slices were drop-fixed in 4% paraformaldehyde in 0.1M PB overnight. Slices were washed in 0.1M PB (3 X 15 minutes) and permeabilized / blocked in 0.5% Triton X-100/10% goat serum in 0.1M PB for at least 2 hours at room temperature. For combined biocytin recovery and immunocytochemistry an initial incubation (4ºC for 40 hours) in primary antibodies diluted at 1:1000 was performed (rabbit anti-PV, Abcam Cat No: ab11427; guinea-pig anti-RFP, SYSY, Cat No: 390005). Slices were washed in 0.1M PB at room temperature 4 X 30 minutes and incubated in secondary antibodies (1:1000 for goat anti guinea-pig Alex-flour 555, Thermofisher Cat No. A21435; 1:500 for goat anti-rabbit Alexa-flour 647, Thermofisher Cat No. A32733 and 1:1000 Streptavidin Alexa FluorTM 488; Thermofisher S1123) overnight at 4oC. After a final wash procedure (4 X 30 minutes) the slices were mounted on microscope slides with Prolong Gold antifade (Thermofisher; Cat No. P36930) for subsequent confocal microscopy.

Immunohistochemistry. Citations with validation data for each antibody are reported on the providers' websites. All animals injected with the virus were transcardially perfused with 4% paraformaldehyde (PFA). The brains were placed in 4% PFA overnight then sectioned at 50 µm using a Leica VTS1000 vibrosector. Floating sections were permeabilized with 0.1% Triton X-100 and PBS for 30 min, washed three times with PBS and incubated in blocking buffer (5% normal donkey serum in PBS) for 30 minutes. The sections were then incubated overnight in blocking buffer with the indicated combination of the following primary antibodies at 4 °C: chicken anti-GFP at 1:1,000 (Abcam USA, ab13970); rabbit anti-DsRed at 1:1,000 (Clontech USA 632496); goat anti-PV at 1:1,000 (Swant USA, PVG-213); guinea-pig anti-PV at 1:1,000 (Swant USA, GP-72); rabbit anti-SST at 1:2000 (Peninsula USA, T-4103.0050); mouse anti-Synaptotagmin-2 at 1:250 (ZFIN USA, #ZDB-ATB-081002-25). The sections were then washed three times with PBS, incubated with Alexa Fluor-conjugated secondary antibodies at 1:1000 (Invitrogen, USA), counterstained with DAPI (Sigma, USA) and mounted on glass slides using Fluoromount-G (Sigma, USA). The staining of PV IHC within human brain tissues was highly variable. As such, estimates of viral specificity were made within regions of cortex and subiculum where staining density was reflective of the known distribution and density of these cells. Given this variability accurate quantitation was not possible.

In-situ hybridization. The in-situ hybridization probes (Gad1; product #400951, Pvalb; product #421931, VIP; product #415961) used were designed by Advanced Cell Diagnostics (Newark, CA, USA). The reagents in the RNAscope® Multiplex Fluorescent Reagent Kit v2 (product # 323100), RNAscope® Probe Diluent (product #300041), HybEZ™ oven (product #321710/321720), humidity control tray (product # 310012), and HybEZ Humidifying Paper (product #310025) were also from Advanced Cell Diagnostics. TSA Plus Fluorescein, TSA Plus Cyanine 3, and TSA Plus Cyanine 5 from PerkinElmer (#NEL741, #NEL744, and #NEL745). Brain tissue was processed as mentioned in the immunohistochemistry section. Brain sections were washed one time in PBS followed by three washes in 0.1% Triton X-100 and PBS, mounted on Superfrost Plus glass slides (Fisher Scientific, 12-550-15) and baked at 60C in the HybEZ oven for 25 minutes. The slides were then submerged in 4% PFA for 30 minutes then washed 3 times in H2O. RNAscope H2O2 was applied to each section for 5 minutes at room temperature. The slides were then washed 3 times in H2O before being submerged in pre-warmed 90ºc H2O for 15 seconds and followed by pre-warmed 90C RNAscope Target Retrieval for 15 minutes. Slides were washed 3 times in H2O before RNAscope Protease III was applied onto each section and then incubated for 15 minutes at 40ºc in the HybEZ oven. Slides were washed 3 times in H2O and then incubated with probe solution diluted to 1:50 with probe diluent for 2 hours at 40ºc in HybEZ oven. Next, the sections were washed three times in RNAscope wash buffer followed by fluorescence amplification. Of note, probes against the RNA of the reporter revealed a non-specific staining that we speculate comes from the viral DNA. In order to reveal the viral reporter, we followed the RNAscope protocol with an IHC amplification of the dTomato. The sections were incubated in blocking solution (0.3% Triton X-100 plus 5% normal horse serum in PBS) for 30 minutes. Then sections were incubated in antibody solution (0.1% Triton X-100 plus 5% normal horse serum in PBS) with rabbit anti-DsRed at 1:250 (Clontech USA 632496) at 4ºc overnight. The sections were then washed three times with PBS, incubated with Alexa Fluor-conjugated secondary antibodies at 1:500 (Invitrogen, USA), counterstained with DAPI (Sigma, USA) and mounted on glass slides using Fluoromount-G (Sigma, USA).

Quantifications and statistics. For strength of expression, fluorescence images were taken at a standardized magnification and exposure time and the average pixel intensity of the cells bodies of each cell expressing the viral reporter was recorded and reported as an average over all cells per enhancer. For quantification of colocalization, cells expressing the indicated reporter were counted using only the corresponding color channel, and then among these cells, the number of cells co-expressing the marker of interest were counted. A cell was considered to be positive for a given marker if the corresponding signal was above background fluorescence. The ratio of cells co-expressing both markers over the total number of cells expressing only the reporter was then calculated, reported here as mean ± s.e.m. Quantifications were performed using a minimum of two independent biological replicates (see supplementary table 1). Several sections from the same animal were used when indicated. Data collection and analysis were not performed blind to the conditions of the experiments, but experimenters from different research groups performed the quantification. No statistical methods were used to predetermine sample sizes, but our sample sizes are similar to those reported in previous publications.

Data availability statement. The data that support the findings of this study are available from the corresponding author upon reasonable request. All AAV plasmids and their corresponding sequences will soon be available on Addgene.

Funding and acknowledgements

IRP of NINDS and a Eunice Kennedy Shriver NICHD Intramural Grant awarded to CJM. JS is supported by National Institute of Neurological Disorders and Stroke Grant No. K99 NS106528. G.F. is supported by NINDS grants NS081297, NS074972, NIMH grant MH071679 and NIH grant UG3MH120096, the Harvard's Dean Initiative, as well as support from the Simons Foundation Award 566615. J.D is supported by NIH grants R01-MH111529 and UG3MH120096, as well as support from the Simons Foundation Award 566615 and a gift from the Friends Of FACES foundation. We are indebted to all of patients who have selflessly volunteered to participate in this study